

## **OPTICAL, STRUCTURAL AND MORPHOLOGICAL CHARACTERIZATION OF $CuIn_{0.7}Ga_{0.3}(Se_{0.6}Te_{0.4})_2$ THIN FILMS UNDER DIFFERENT ANNEALING TEMPERATURES**

**Songül FİAT VAROL<sup>1</sup>, Emin BACAŞIZ<sup>2</sup>, Güven ÇANKAYA<sup>3</sup> and Michael KOMPİTSAS<sup>4</sup>**

<sup>1</sup>Dumlupınar University, Technology Faculty, Energy Systems Engineering, 43500 Kütahya, TÜRKİYE

<sup>2</sup>Karadeniz Technical University, Faculty of Arts and Sciences, Physics Department, 61080 Trabzon, TÜRKİYE

<sup>3</sup>Yıldırım Beyazıt University, Faculty of Engineering and Natural Sciences, Materials Engineering, 06030 Ankara, TÜRKİYE

<sup>4</sup>National Hellenic Research Foundation, Theoretical and Physical Chemistry Institute, 11635 Athens, GREECE

**Abstract:**  $CuIn_{0.7}Ga_{0.3}(Se_{0.6}Te_{0.4})_2$  (CIGSeTe) thin films have been deposited by e-beam evaporation system. The optical measurements have been carried out in the wavelength range 300–1200 nm. The films have high absorption and optical band gaps ranging from 1.15, 1.12, 1.11, 1.06 and 1.05 eV according to the as deposited and annealing temperatures subsequently as deposited, 450 °C, 475 °C, 500 °C, and 525 °C. The obtained polycrystalline CIGS films showed the chalcopyrite structure with predominant growth in the (1 1 2) direction. The linear dependence of the lattice parameters as a function of Se and Te contents were examined. The lattice parameter were determined as  $a = 6.00 \text{ \AA}$  and  $c = 11.85 \text{ \AA}$  for as deposited films and  $a = 6.07 \text{ \AA}$  and  $c = 12.09 \text{ \AA}$  for annealed films at higher temperature 525 °C. The surface map exhibited a compact and a granular morphology depending on the composition with SEM images. Also AFM images verify this better crystallization with bigger grains that roughness varied from 12.10 to 14.82 nm rms (root mean square) values.

**Keywords:** CIGS, Optical characterization; XRD; AFM; SEM.

## **$CuIn_{0.7}Ga_{0.3}(Se_{0.6}Te_{0.4})_2$ İNCE FİMLERİN FARKLI TAVLAMA SICAKLILARI ALTINDA OPTİK, YAPISAL VE MORFOLOJİK KARAKTERİZASYONU**

**Özet:**  $CuIn_{0.7}Ga_{0.3}(Se_{0.6}Te_{0.4})_2$  (CIGSeTe) ince filmleri e-demeti ile buharlaştırma sistemi ile elde edildi. Optik ölçümler 300–1200 nm dalgaboyu aralığında alınmıştır. Filmler yüksek soğurma gücüne ve sırasıyla tavlama sıcaklıklarına göre 1.15, 1.12, 1.11, 1.06 ve 1.05 eV band aralıklarına sahiptir. Elde edilen polikristal yapıdaki filmler (1 1 1) baskın yönelimi ile kalkoprit karakteristiği göstermiştir. Se ve Te içeriğinin bir fonksiyonu olarak örgü parametrelerinin lineer bağımlılığı tespit edilmiştir. Tavlama sıcaklıklarına göre örneklerin örgü parametreleri  $a = 6.00 \text{ \AA}$  ve  $c = 11.85 \text{ \AA}$  olarak, 525 °C de tavlama sıcaklığına göre ise  $a = 6.07 \text{ \AA}$  ve  $c = 12.09 \text{ \AA}$  olarak belirlenmiştir. Bileşime bağlı olarak oluşumun yüzey haritası SEM görüntülerinde kompakt ve tanecikli bir yapı sergilemiştir. Ayrıca, AFM görüntüleri de bu daha iyi olan kristalleşmeyi daha büyük taneciklerle ve 12.10 den 14.82 nm'ye değişen rms pürüzlülük değerleri ile doğrulamaktadır.

**Anahtar Kelimeler:** CIGS; Optik Karakterizasyon; XRD; AFM; SEM.

## 1. INTRODUCTION

The efficiency of polycrystalline thin film solar cells based on  $\text{Cu}(\text{In,Ga})\text{Se}_2$  (CIGS) has approached 19% [1]. Thin layers of  $\text{CuIn}_x\text{Ga}_{1-x}\text{Se}_2$  are considered to be the most suitable materials for high efficiency solar cells because of their high absorption coefficient ( $<10^5 \text{ cm}^{-1}$ ), direct band gap and stability against photo-degradation. The  $\text{CuIn}_{1-x}\text{Ga}_x\text{Se}_2$  quaternary alloy is a semiconductor with the gap energies varying from 1 eV (for  $x = 0$ ) to 1.7 eV (for  $x = 1$ ); thus it allows tailoring of optical band gap for optimum solar cell conversion [2, 3].

In this research, we report the structural properties and surface topography of  $\text{CuIn}_{0.7}\text{Ga}_{0.3}(\text{Se}_{0.6}\text{Te}_{0.4})_2$  (CIGSeTe) thin film fabricated by electron beam evaporation technique. Among the PVD techniques, electron beam evaporation offers significant advantages in terms of high directionality, stoichiometry and purity of the films. Analogous to flash evaporation, in electron beam evaporation, high thermal density prevailing over a small region of the source ensures complete evaporation of material without preference to the vapour pressures of the individual elements. This also eliminates the secondary process of selenization usually observed in the preparation of CIGS films by other methods [4,5]. Incorporation and adjustment of gallium concentration in the absorber layer of  $\text{Cu}(\text{InGa})\text{Se}_2$  to a suitable value enhances the collection of photo-generated carriers [6]. But attempts to achieve high efficiencies using  $[\text{Ga}]/([\text{In}] + [\text{Ga}])$  ratio greater than 0.3 have failed as the open circuit voltage does not proportionally increase with the band gap energy [7]. The content of Ga in a CIGS absorber layer basically confines its functional properties and its applicability as a photovoltaic material. When Ga is in excess of 30%, (or In is less than 70%), the CIGS segregates into CIS and CGS.

Here we report our attempts to explore the feasibility of growing high quality  $\text{CuIn}_{0.7}\text{Ga}_{0.3}(\text{Se}_{0.6}\text{Te}_{0.4})_2$  films using electron beam evaporation method. Also, we present our studies on structural, surface and optical properties of CIGSeTe films with a view to deriving meaningful information on the effect of both Se and Te existence in CIGSeTe films with increasing annealing process. So both Te presence and annealing temperature effect can be evaluated on CIGS thin films with derived parameters to use as photovoltaic devices.

## 2. EXPERIMENTAL PROCEDURE

$\text{CuIn}_{0.7}\text{Ga}_{0.3}(\text{Se}_{0.6}\text{Te}_{0.4})_2$  has been prepared by using five different elements such as, copper (Cu), indium (In), gallium (Ga) selenium (Se) and tellurium (Te). Stoichiometric amounts of the individual elements: copper, indium, gallium, selenium and tellurium according to the required compositions are placed in a quartz ampoule, coated inside with carbon in order to prevent a reaction between elements and the walls of ampoule as well as to avoid their contamination [8]. The ampoule is evacuated down to a pressure of  $\sim 2.10^{-6}$  Torr and then sealed-off. The quartz ampoule with the mixture of elements is placed in a furnace which is heated at a rate of  $100^\circ\text{C}$  per hour ( $^\circ\text{C}/\text{h}$ ) in steps up to  $1100^\circ\text{C}$  and kept at this temperature for 24 hours. The quartz ampoule is then allowed to cool slowly at rate of  $100^\circ\text{C}/\text{h}$  to room temperature. In order to homogenize the molten mixture, during the process of heating and cooling, the ampoule is vibrated constantly.

Before deposition, soda lime glass (SLG) substrates were well cleaned to avoid the impurity formations between the film and the substrate. They were first cleaned with a detergent solution to get rid of the gross dirt existing on the surface. Then this process was repeated at about  $60^\circ\text{C}$  by using an ultrasonic cleaner. The glass slides were then flushed with distilled water and boiled in a solution

of 30 % H<sub>2</sub>O<sub>2</sub> to remove the organic materials on the surface. Finally, the slides were rinsed with the hot water in the ultrasonic cleaner. The substrates, after the cleaning process, were kept in methanol and were dried by pure nitrogen before deposition.

The deposition process takes place inside the vacuum chamber which was first evacuated to 133 mPa by a mechanical pump and then to ~133 iPa by a turbo molecular pump. CIGSeTe thin films were grown on the substrates by applying electron beam (e-beam) evaporation. In this method, the CIGS polycrystalline target was placed in the crucible and the electron beam, created by a filament, was accelerated and focused and by a permanent magnet onto the target. The kinetic energy of the electrons bombarding the target is transformed into thermal energy. The increasing surface temperature of the target results in the formation of a liquid melt, the material evaporates under vacuum and condensates on the substrate. The temperature was set at 300°C before the thin films evaporation process. After growth the films were annealed at different temperatures in argon ambient at a pressure of 10<sup>5</sup> Pa, upon a flushing process: first the chamber was exposed to vacuum and then the chamber was filled with high purity argon gas.

In this study, thin film thicknesses varied from 870 nm to 890 nm with annealing, measured by ellipsometry.

### 3. RESULTS AND DISCUSSIONS

#### 3.1 Structural Properties (XRD)

Fig. 1 shows the X-ray diffractometry (XRD) pattern of the sample evaporated with e-beam. In the XRD measurements, the grazing incidence angle is 0.2° and the diffraction angles are scanned from 20 to 70°.

In the XRD patterns, the most intense peak at 26.7° 2θ indicates the stoichiometric CIGS alloy has a (112) orientation. The other

prominent peaks correspond to the (2 0 4)/(2 2 0) and (1 1 6)/(3 1 2) phases. In addition to these peaks commonly observed in CIGS, (041) orientation was also present in the XRD patterns. The lattice parameters, 'a=b' and 'c' for the films were calculated as 6.00, 11.85 Å for not annealed and 6.07, 12.09 Å for annealed film at 525 °C respectively. At the same time, grain sizes were calculated as 69.53 for not annealed and 75.62 for annealed film at 525 °C (Table 1) with Bragg's Law and Scherrer Formula [9].

Annealing crystallizes the films and also result the phase segregation as seen in the XRD spectra of the thin films shown in Fig. 1. On increasing the annealing (525 °C) the secondary phases Cu<sub>2</sub>Se and Cu<sub>3</sub>In<sub>5</sub>Se<sub>9</sub> dissociated and the corresponding peak intensity was suppressed in the XRD spectra. This behaviour has been reported earlier by refs. [10,11]. Annealing also suppresses the (1 1 6)/(3 1 2) and (2 0 4)/(2 2 0) doublet of CIGS phases. The presence of diffraction peaks corresponding to CIGS chalcopyrite structure confirms the formation of a single phase microstructure. Prolonged ageing at either of these temperatures does not result in any significant changes as reported by ref. [11].

Annealing at low temperature enables that diffusion (phase segregation) and crystallization occur simultaneously. It is suspected that the Cu<sub>2</sub>Se phase forms on the surface and the grain boundaries [12]. Annealing at 525 °C thus improves crystallinity, constrains diffusion pathways for compound formation, dissociates secondary phase and hence increases the overall efficiency of the films.

In ref. [13] have been reported that in the case of chalcopyrite CIGS films the strongest reflexes are the (1 1 2) and the overlapping (2 2 0)/(2 0 4), which correspond to different preferred orientations. Similar observations confirming chalcopyrite phase have been

reported with many studies [10, 14-16]. According to Fig. 1., we can say that heat treatment at 450 °C basically induces diffusion-driven phase segregation resulting in a non-homogenous composition ranging from Cu-rich to Se+Te- rich ( $\text{CuIn}_{0.7}\text{Ga}_{0.3}(\text{Se}_{0.6}\text{Te}_{0.4})_2$ ) and a co-existence of two phases.

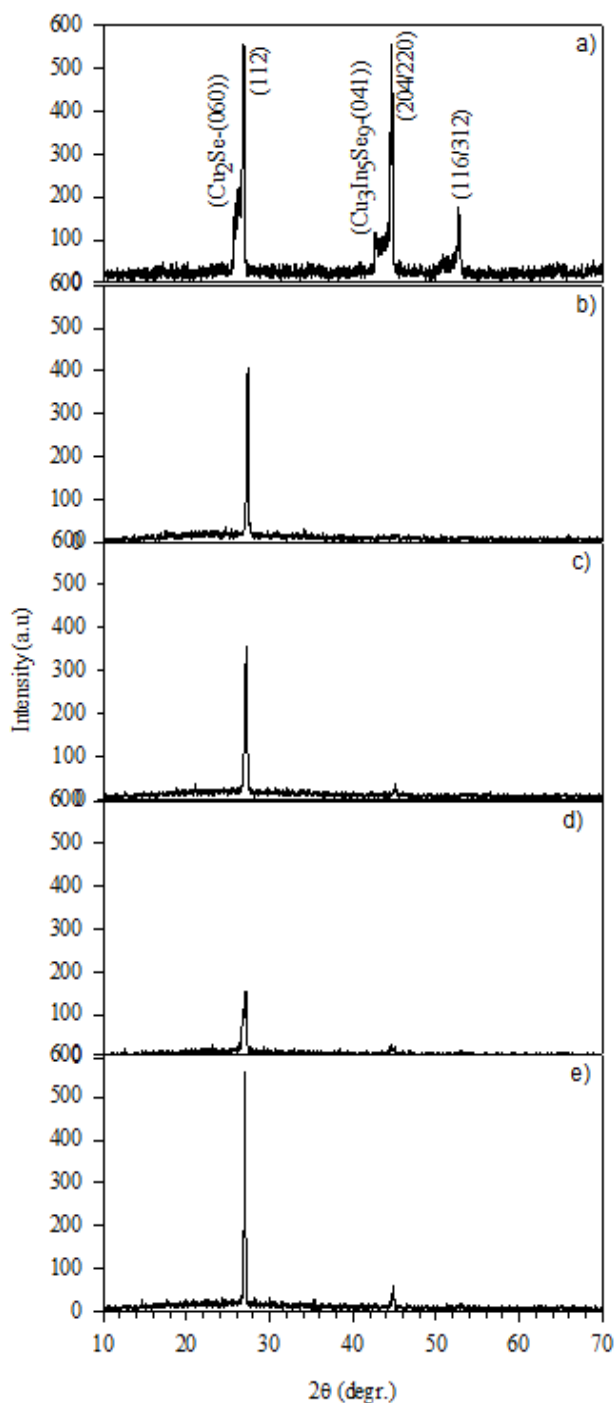


**Fig. 1.** X-ray diffractograms of the  $\text{CuIn}_{0.7}\text{Ga}_{0.3}(\text{Se}_{0.6}\text{Te}_{0.4})_2$  thin films prepared at different annealing temperatures a) As deposited, b) 450 °C, c) 475 °C, d) 500 °C, e) 525 °C

### 3.2 Surface Properties (AFM, SEM)

Our XRD results showed that we caught a chalcopyrite structure for  $\text{CuIn}_{0.7}\text{Ga}_{0.3}(\text{Se}_{0.6}\text{Te}_{0.4})_2$  thin films. This indicates that the stoichiometry of this complicated multinary elemental structure could be achieved in thin film form using electron beam deposition technique. Topographical study on the CIGS thin films have been performed using AFM conducting mode. AFM image of the not annealed film reveals a “small” pellet structure with dense grains (Fig.2).

The surface topography is composed of clusters of varying sizes with irregular shapes. The irregular shape of the grains suggests that for not annealed films, the kinetic energy is not sufficient for the coalescence of the grains. When the film anneals, the crystalline structure and clear grain boundaries became apparent. The rms roughness values of the  $\text{CuIn}_{0.7}\text{Ga}_{0.3}(\text{Se}_{0.6}\text{Te}_{0.4})_2$  films grown as deposited and 525 °C were 12.10 nm and 14.82 nm, respectively.

It confirms the conclusion drawn from the XRD measurements that  $\text{CuIn}_{0.7}\text{Ga}_{0.3}(\text{Se}_{0.6}\text{Te}_{0.4})_2$  film has maximum grain/crystallite size and it increases with annealing process. This phenomenon is probably related to a higher degree of recrystallization of the film at higher heat treatment. Above 500 °C, resulting in the formation of round edged grain structures with a strong (1 1 2) preferred orientation. A typical example of such a film was shown in Fig. 3

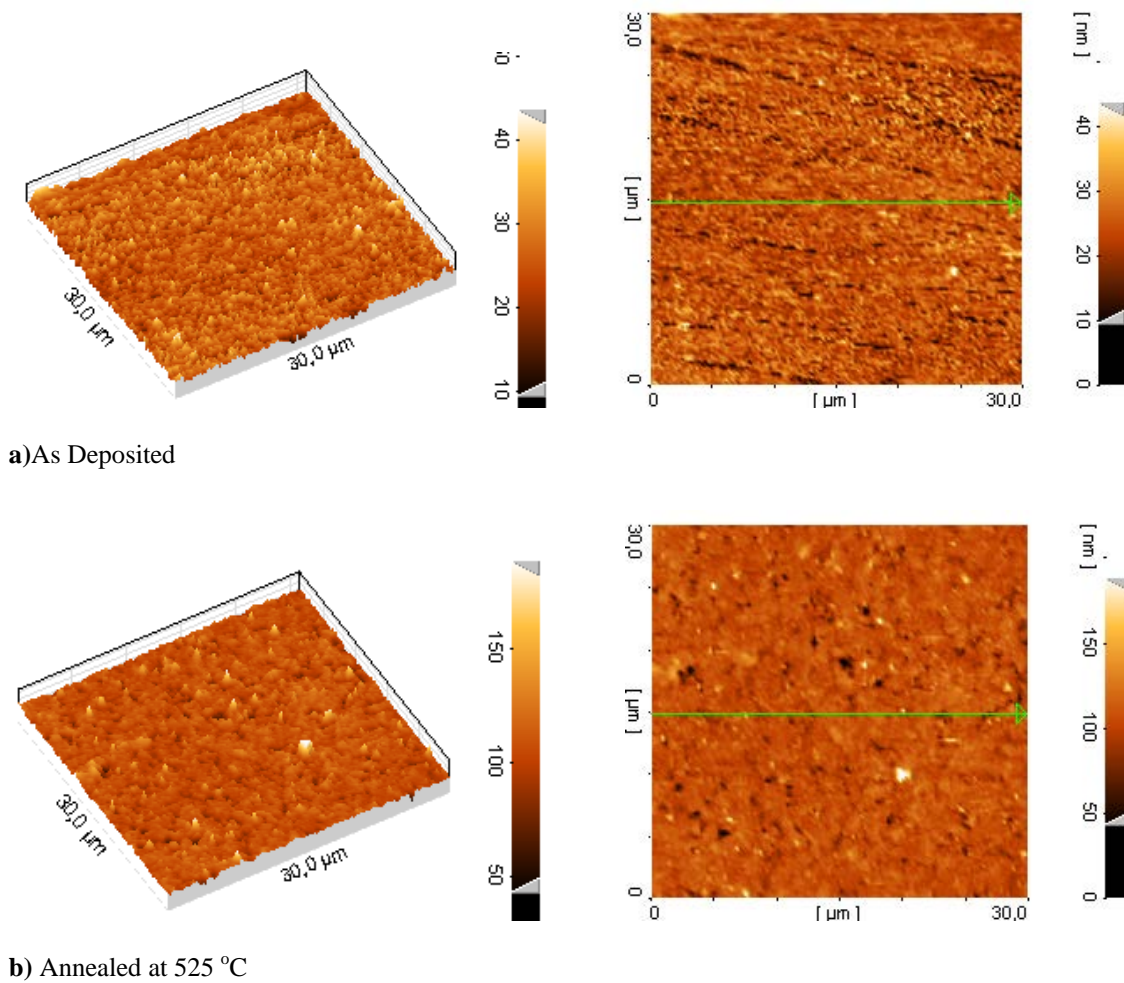
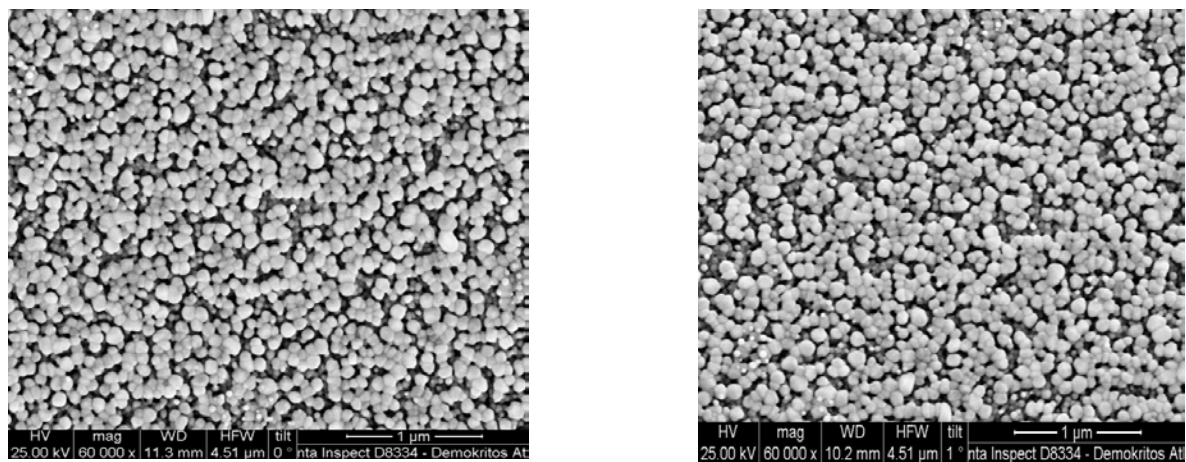


**Fig. 2** AFM images of the  $\text{CuIn}_{0.7}\text{Ga}_{0.3}(\text{Se}_{0.6}\text{Te}_{0.4})_2$  thin films a) As deposited, b) Annealed at 525 °C temperature.



a) As deposited

b) Annealed at 525 °C

**Fig. 3.** SEM images of  $\text{CuIn}_{0.7}\text{Ga}_{0.3}(\text{Se}_{0.6}\text{Te}_{0.4})_2$  for as deposited and annealed at 525°C thin films (X60.000 magn.) a) As deposited b) Annealed at 525 °C

### 3.3 Optical Properties

Transmission spectra, in the wavelength range 300–1200 nm, at normal incidence, of  $\text{CuIn}_{0.7}\text{Ga}_{0.3}(\text{Se}_{0.6}\text{Te}_{0.4})_2$  thin films of thickness 870 nm, deposited at different annealing temperatures, were recorded. From these spectral data, the optical absorption coefficient,  $\alpha$ , was calculated using following equation [17].

$$\alpha = A(h\nu - E_g)^{1/2} \quad (1)$$

where  $h$  is the Planck constant;  $\nu$  is the frequency of the incident photon; and  $A$ , a

constant depending on electron–hole mobility.  $(\alpha h\nu)^2$  versus  $h\nu$  plots were analysed using the Eq. (1). From the plot, the band gap energy was determined by extrapolating the linear part of the graph towards  $h\nu = 0$ . Figure 4 shows the Tauc plots of  $(\alpha h\nu)^2$  versus photon energy  $h\nu$  of  $\text{CuIn}_{0.7}\text{Ga}_{0.3}(\text{Se}_{0.6}\text{Te}_{0.4})_2$  thin films for as deposited and annealed films, respectively.

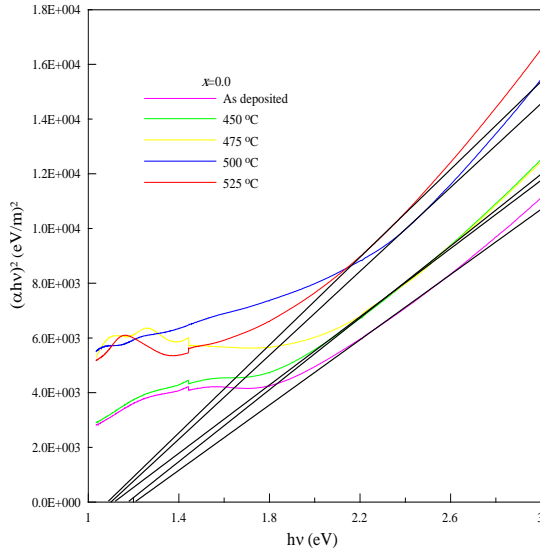


**Fig. 4.** Plots of  $(\alpha h\nu)^2$  versus  $h\nu$  for  $\text{CuIn}_{0.7}\text{Ga}_{0.3}(\text{Se}_{0.6}\text{Te}_{0.4})_2$  thin films deposited at different annealing temperatures.

In the case of e-beam evaporated films, the optical band gap was shifted from 1.15 eV to 1.05 eV after annealing (Table 1). The shift to low-energy values can be explained in terms of the nano-size effect of the as-deposited film. The large shift of optical band gap, however, was not observed in this study. The intensity of transmittance just increased slightly after annealing at short wavelength. The experimental results show that the average value of the optical transmittance is roughly of the order of 70% for the upper part of the spectrum ( $\lambda > 1000$  nm). For shorter wavelengths, the transmittance decays

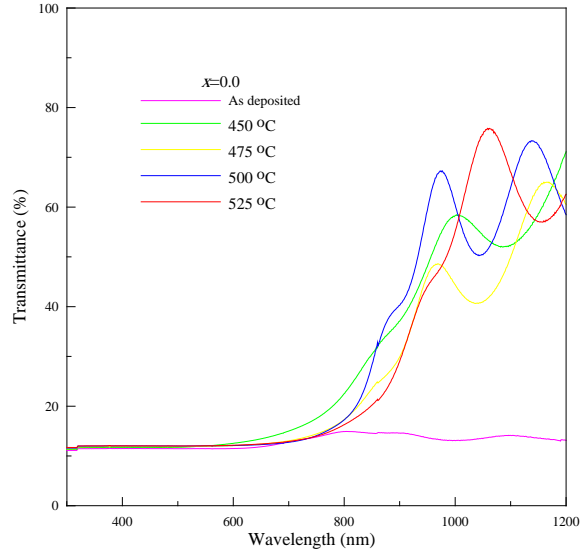


**Fig. 5.** Transmittance curves for  $\text{CuIn}_{0.7}\text{Ga}_{0.3}(\text{Se}_{0.6}\text{Te}_{0.4})_2$  thin films deposited at different annealing temperatures

strongly and it remains practically constant at ~10%, in particular for  $\lambda < 800$  nm (Fig. 5).

All films show low transmission in the region of 700–900 nm. In the range of 900–1200 nm, the transmission of each samples increases rapidly. The low band gap can assist charge separation, but is detrimental in terms of open circuit voltages. On the other hand, although the wide band gap increases open circuit voltages, it blocks photocurrent collection. The ideal band gap is in the range of 1.1–1.15 eV for solar cell applications [18].

It may be attributed to the low light scattering effect for its lower surface roughness. It was reported that for as deposited and annealed  $\text{CuIn}_{0.7}\text{Ga}_{0.3}(\text{Se}_{0.6}\text{Te}_{0.4})_2$  films, direct optical band ranges are in good agreement with other studies [19-22]. This decrease in the energy band gap may be due to reduced strain and dislocation density in films. The literature datas [23, 24] also exhibited a decrease in  $E_g$  with increasing annealing temperature for

different thin films, due to the increase in the energy widths of the band tail states and quantum-size effect and the existence of an amorphous phase. Therefore, it is believed that both the increase in crystallite size and the reduction in amorphous phase amount are responsible for the bandgap decreasing in the annealed  $\text{CuIn}_{0.7}\text{Ga}_{0.3}(\text{Se}_{(1-x)}\text{Te}_x)_2$  films. Also, Shah et al., verified this decreasing with annealing [25].

**Table 1.** The Band gap values, Grain sizes and lattice parameters for  $\text{CuIn}_{0.7}\text{Ga}_{0.3}(\text{Se}_{0.6}\text{Te}_{0.4})_2$  thin films deposited at different annealing temperatures.

Anneal. Temp.(°C)	Band Gap (eV)	Grain Sizes and Lattice parameters (nm, Å°)
As deposited	1,15	69.53 a:6.00 c:11.85
450	1,12	69.00 a:6.01 c:11.76
475	1,11	69.87 a:6.01 c:11.92
500	1,06	73.52 a:6.03 c:12.13
525	1,05	75.62 a:6.07 c:12.09

According to these results, we concentrate on both the crystallization and the reduction of the amorphous phase, are responsible for the band gap decrease of the annealed CIGSeTe films in this work to catch the best performance of this structure for solar cell applications.

#### 4. Conclusions

In this study, chalcopyrite CIGSeTe thin films were fabricated by e-beam evaporation of Cu–In–Ga–Se–Te five metallic precursors.  $\text{CuIn}_{0.7}\text{Ga}_{0.3}(\text{Se}_{0.6}\text{Te}_{0.4})_2$  thin films have been examined as deposited and annealed samples have been found to be polycrystalline in nature with chalcopyrite phase. The films annealed from 450 to 525 °C showed the chalcopyrite with Se+Te, it has better crystalline quality and proper band gap for

solar cell applications than those as deposited films. Also, the crystalline nature has been observed to improve with annealing temperature. The AFM studies confirm that the roughness of the CIGSeTe films increases with annealing that can be attributed to their atomic radius magnitudes and choosing high annealing temperature. Also film thicknesses varied from 870 nm to 890 nm with annealing. Band gaps have been found in the expected range from 1.15eV to 1.05 eV that this kind of films that can be evaluated as different alternative absorbers in photovoltaic for CIGS-based thin film solar cells using Te.

#### Acknowledgements

This work is supported by Gaziosmanpaşa University Scientific Research Project (BAP) with the Grand Contract No: 2010/12.

## References

- [1] Contreras M.A., Egaas B., Ramanathan K., Hiltner J., Swartzlander A., Hasoon F., Noufi R., 1999. Prog. Photovolt. Res. Appl. 7, 311.
- [2] Bhattacharya R.N., Contreras M.A., Egaas B., Noufi R.N., 2006. App. Phys. Lett. 89, 253503.
- [3] Ramanathan K., Teeter G., Keane J.C., Noufi R., 2005. Thin Solid Films 480, 499.
- [4] Klenk, R., Bakehe, S., Kaigawa, R., Neisser, A., Reib, J., Lux-Steiner, M.Ch., 2004. Thin Solid Films 424, 451–452.
- [5] Sakurai, K., Hunger, R., Suchimochi, N., Baba, T., Matsubara, K., Fons, P., Yamada, A., Kojima, T., Deguchi, T., Nakanishi, H., Niki, S., 2004. Thin Solid Films 6,431–432.
- [6] Boslo, A., Romeo, N., Podesta, A., Mazzamuto, S., Canevari, V., 2005. Cryst Res Tech, 40, 1048.
- [7] Papadimitriou, D., Esser, N., Xue, C., 2005. Physica Status Solidi 242, 2633.
- [8] Fiat S., Koralli P., Bacaksiz E., Giannakopoulos K.P., Kompitsas M., Manolakos D.E., Çankaya G., 2013. Thin Solid Films 545,64–70.
- [9] Aissaoui O., Bechiri L., Mehdaoui S., Benslim N., Benabdeslem M., Portier X., Lei H., Doualan J.L., Nouet G., Otmani A., 2009. Thin Solid Films 517, 2171–2174.
- [10] Bouabid, K., Ihlal, A., Manar, A., Outzourhit, A., Ameziane, E.L., 2005. J Phys, IV France 123, 53.
- [11] Bouabid, K., Ihlal, A., Manar, A., Outzourhit, A., Ameziane, E.L., 2005 Thin Solid Films 448, 62.
- [12] Keyes, Brian M., Dippo, P., Metzger, W., Abushama, J., Noufi, Rommel, 2002. Proceedings of 29th IEEE Photovolt Specialists Conference 1.
- [13] Virtuani A., Lotter E., Powallia M., 2006. J. Appl. Phys 99, 014906.
- [14] El Haj Mousa, G.W., Ajaka, M., El Tahchi, M., Eid, E., Llenares, C., 2005. Phys Stat Solidi (a) 202, 469.
- [15] Fahoume, M., Boudarine, H., Aggour, M., Chraïbi, F., Ennaoui, A., Delplancke, J.L., 2005. Journal of Physics, IV France 123, 75.
- [16] Calixio, M.E., Bhattacharya, R.N., Sebastian, P.J., Fernandez, A.M., Gamhua, S.A., Noufi, R.N., 1998. Sol. Energy Mater. Sol. Cells 55, 23.
- [17] Tauc J. C., Amorphous and liquid semiconductor, New York: Plenum Press. (1974) p. 159.
- [18] Zegadi A., Slifkin M.A., Djamin M., Hill A.E., Tomlinson R.D., 1992. Phys Stat Solidi (a) 133, 533.
- [19] Romeo A., Terheggen M., Abou-Ras D., Batzner D.L., Haug F.J., Kalin M., Rudmann D., Tiwari A.N., 2004. Prog. Photovolt.: Res. Appl. 12, 93–111.
- [20] Kemell M., Ritala M., Leskela M., 2005. Solid State Mater. Sci. 30, 1–31.
- [21] Guillemoles J.F., Cowache P., Massaccesi S., Thouin L., Sanchez S., Lincot D., Vedel J., 1994. Adv. Mater. 6, 379–381.
- [22] Malar P and Kasiviswanathan S., 2005. Sol. Energy Mater. Sol. Cells 88, 281–292.
- [23] Bao D. and Yao X., 2001. Appl. Phys. Lett. 79, 3767.
- [24] Colakoglu, T., Parlak M., Ozder S., 2008. J of Non-Cryst Solids, 354, 3630–3636.
- [25] Shah N.M., Panchal C.J., Kheraj V.A., Ray J.R., Desai M.S. 2009. Solar Energy 83, 753–760.

**Geliş Tarihi:12.02.2013**

**Kabul Tarihi:27.09.2013**